Spatially Resolved Degradation of Solar Modules in Dependence of the Prevailing Microclimate

Robert Heidrich, Anton Mordvinkin, and Ralph Gottschalg

***Abstract*—In this work, a holistic approach to analyze solar module degradation is undertaken. The degradation kinetics of UV additives in the ethylene-vinyl acetate copolymer (EVA) encapsulant are derived using a quantification method. In addition, minimodules are analyzed after combined accelerated aging (UV irradiation at 85°C and 60% relative humidity) at different positions. In this way, the local degradation reactions of the encapsulant are determined as a function of the prevailing stressors and additive consumption. These findings are correlated with the electrical characterization ($I - V$ and electroluminescence measurements) to expand the understanding of module degradation. Performance losses are mainly due to a combination of hydrolysis and Norrish type II reactions of the encapsulant, as acetic acid is produced in both cases corroding the electrical contacts. Independent of the local stressor, the UV stabilizer shows first-order degradation kinetics, which is directly linked to the degradation of the encapsulant and, thus, indirectly to cell degradation. It is shown that the UV stabilizer consumption is an early precursor of module degradation and could be utilized to evaluate the remaining lifetime of a PV module.**

***Index Terms*—Additives, degradation, encapsulant, ethylene-vinyl acetate copolymer (EVA), performance loss, spectroscopy.**

I. Introduction

SOLAR energy has become one of the most important energy sources of our time and will continue its success story in the near future [1]. Reliability and lifetime of the components are nowadays the main factors determining the costs of energy. There are several approaches to predict the long-term behavior of PV modules [2], [3], [4], [5], [6]. However, these are generally empirical without consideration of the underlying degradation mechanisms of the individual components of a module [2], [3], [4], [5].

The packaging materials used for solar modules determine their long-term behavior [7], [8], [9], [10]. In particular, the interaction of the individual encapsulant layers with the backsheet can have an influence on the degradation behavior of the modules [6], [11]. The additives contained in the various polymer layers, in turn, determine the degradation behavior of these layers [12], [13], [14]. In the end, an understanding of additive and polymer degradation and its influence on the degradation of the solar cell and the electrical connectors is essential for the development of a physics-based degradation model.

There is a large body of work dealing with the degradation of ethylene-vinyl acetate copolymer (EVA) [13], [14], [15], [16], [17], [18], [19], [20], [21], which is currently the most widely used encapsulant. There are also various studies on the degradation of different backsheets [22], [23], [24]. However, these materials are often only studied in isolation, although the degradation behavior in combination, especially with a solar cell, can be completely different. This can be explained by the fact that different microclimates occur within a PV module. Certain parts are more exposed to moisture than others and UV radiation does not reach all areas to the same extent. In addition, mobile species such as polymer additives can diffuse within or between the different layers [14]. Degradation effects such as PID are also heavily dependent on the combination of materials used [25], [26]. It is, therefore, to be expected that different degradation reactions take place depending on the position in a solar module.

The dependence of the degradation kinetics on the prevailing microclimate leads indirectly to the next problem. In most studies and weathering standards in the field of accelerated aging, a distinction is usually made between UV aging and damp heat (DH) aging [13], [14], [21], [27], [28], [29], [30]. Considering the different climatic conditions around the world, it is unrealistic to expose material combinations to only one type of stressor at a time. Although there has been some recent work in this direction, which has shown that field failures can be provoked, much research still needs to be done to develop optimal aging procedures [31], [32], [33].

This work is intended to investigate the influence of these microclimates, which arise under combined weathering conditions. It is an extension of our previously published work [34]. For this purpose, minimodules were produced in a conventional structure and aged at an accelerated rate. In addition, pure EVA films were weathered in the same chamber. Using a recently developed method for UV additive quantification, the degradation kinetics of UV absorber and UV stabilizer in EVA are to be derived [35]. Afterward, the additive consumption of the pure EVA films is compared with those in the module, enabling the correlation of UV additive degradation with the aging of the encapsulant and macroscopic effects, such as module performance. The minimodules are examined at different positions using Fourier-transform infrared spectroscopy (FTIR)

Manuscript received 11 March 2024; revised 14 April 2024; accepted 7 June 2024. Date of publication 21 June 2024; date of current version 26 August 2024. This work was supported by TotalEnergies. *(Corresponding author: Robert Heidrich.)*

Robert Heidrich and Ralph Gottschalg are with the Fraunhofer Center for Silicon Photovoltaics CSP, 06120 Halle, Germany, and also with the Anhalt University of Applied Sciences, 06366 Koethen, Germany (e-mail: robert.heidrich@csp.fraunhofer.de; ralph.gottschalg@csp.fraunhofer.de).

Anton Mordvinkin is with the Fraunhofer Center for Silicon Photovoltaics CSP, 06120 Halle, Germany (e-mail: anton.mordvinkin@csp.fraunhofer.de).

Color versions of one or more figures in this article are available at https://doi.org/10.1109/JPHOTOV.2024.3414179.

Digital Object Identifier 10.1109/JPHOTOV.2024.3414179

to analyze the effect of the respective microclimate on the degradation reactions of the encapsulant. These are correlated to the electrical characterization of the modules to understand the degradation chain.

II. Materials and Methods

A. Minimodules

The single-cell minimodules used correspond to the conventional structure of a solar module with the dimension of approximately 20 cm × 20 cm. The front sheet used was 3-mm float glass. The EVA has a UV cut-off (50% transmittance at 365 nm), a vinyl acetate (VA) content of 26%–28%, and a thickness of 0.4–0.6 mm. The light transmission is reported to be over 91% by data sheet and the EVA was used as the encapsulation material for the front and back sides. A Meier ICOLAM 10/08 was used for lamination with the following parameters: The laminator was set to 55 °C. The samples were then placed in the laminator, which was evacuated for 6.5 min and heated to 80 °C. The modules were then pressed with 600 mbar and heated to 155 °C within 3 min. The temperature and pressure were maintained for a further 15 min. Finally, the laminator was cooled down to 55 °C within 30 min while the pressure of 600 mbar was kept constant. The gel content after lamination is specified in the data sheet with over 85% while measurements of separate films show gel contents of around 90%. This means that no remaining crosslinking peroxides are to be expected. The entire lamination process complies with the manufacturer's specifications for the EVA used. The solar cells are based on PERC technology with five busbars and four electrical contacts for $I-V$ measurements. The backsheet is based on polyethylene terephthalate (PET) with a thickness of 320 μm. The moisture permeability of the backsheet is specified with 1.9 g/m^2 per day. After lamination, the edges of the minimodules were sealed with an aluminum tape to simulate a frame and make it more difficult for moisture to penetrate while reducing edge effects.

B. Sample Preparation

For the measurements with pure EVA, an approx. 30 cm × 30 cm piece of film was laminated under the abovementioned conditions. Subsequently, 5 cm × 5 cm squares were cut out and aged in the climate chamber. Two film samples were available for each weathering step. For the PY-GCMS measurements, samples weighing approximately 4 mg (2–3 mm in diameter) were punched out. Consequently, the complete bulk was always measured in order to exclude surface effects. The PY-GCMS measurements were carried out in triple determination.

Sampling of the minimodules was carried out at various points in order to analyze aging effects in a spatially resolved manner. The different positions are shown in Fig. 4. The following nomenclature is used throughout the paper: t_r_f—front EVA on top of the inner interconnector at the top of the module, b_r_f—front EVA on top of the inner interconnector at the back of the module, m_m_b—back EVA in the middle of the module. For the b_r_f and t_r_f samples, the backsheet was cut in the area of the inner interconnector. Afterward, the interconnector was removed as a whole from the module. The front EVA remained on the glass and could be removed with a scalpel. For the m_m_b position, the backsheet was carefully removed layer by layer with a scalpel until the EVA layer on the back was visible. This was also carefully prepared with the scalpel to avoid contamination by the solar cell. PY-GCMS and FTIR measurements of the minimodules were carried out in double determination.

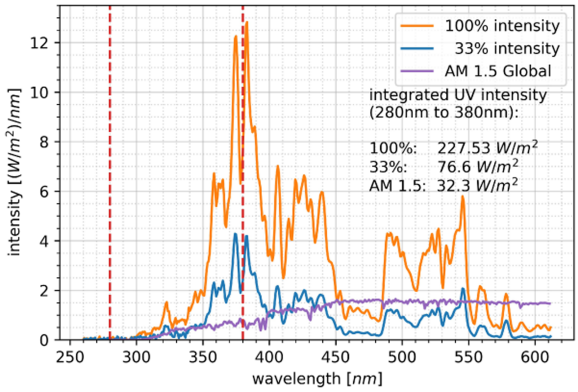

Fig. 1. Spectrum of the used metal halide lamps in comparison with the AM 1.5 global (ASTM G173-03 reference spectra derived from SMARTS v. 2.9.2. provided by NREL). The 100% weathering corresponds to the intensity used in our previous work [34].

C. Weathering

The weathering was carried out in CTS CSL −70/1500 UV climate chambers and was based on IEC 61215, but the parameters were varied [29]. A combination of DH and UV conditions was selected. The temperature was set to 85 °C and the relative humidity (r.h.) to 60%. The irradiation was realized by metal halide lamps, which were set with an integrated irradiance of 76.6 W/m^2 (33% weathering—this work) and 227.53 W/m^2 (100% weathering—previous work for comparison [34]) between 280 and 380 nm. The spectrum used is shown in Fig. 1, especially in the high-energy UV range, it is similar to the AM 1.5 global. The minimodules produced were weathered for a maximum of 2000 h. The electrical characterization was carried out every 250 h for all modules. After each weathering step, two modules were removed for destructive measurement procedures.

Temperature measurements at various positions inside modules with a comparable structure (same glass, same cell type, same encapsulant, and white backsheet) under the same weathering conditions show that the area below the solar cell reaches approximately 90 °C while b_r_f and t_r_f positions reach approximately 88 °C. Additionally, previous studies with xenon lamps have shown that the sample temperature of clear and white samples can be approximated by the chamber temperature during UV weathering [36], [37]. Thus, the temperature of the plain EVA films can be approximated by the chamber temperature.

D. Characterization Methods

1) I–V Characterization and Electroluminescence (EL) Measurements: The $I-V$ characteristics were measured with a Berger Lichttechnik solar simulator (Flasher system). The tests were carried out at 25 °C and an irradiance of 1000 W/m^2 (standard test conditions). The flasher corresponds to class A in the categories of homogeneity, spectral consistency, and temporal stability. The repeatability is less than 0.3% deviation. The flasher was calibrated with a reference module before each series

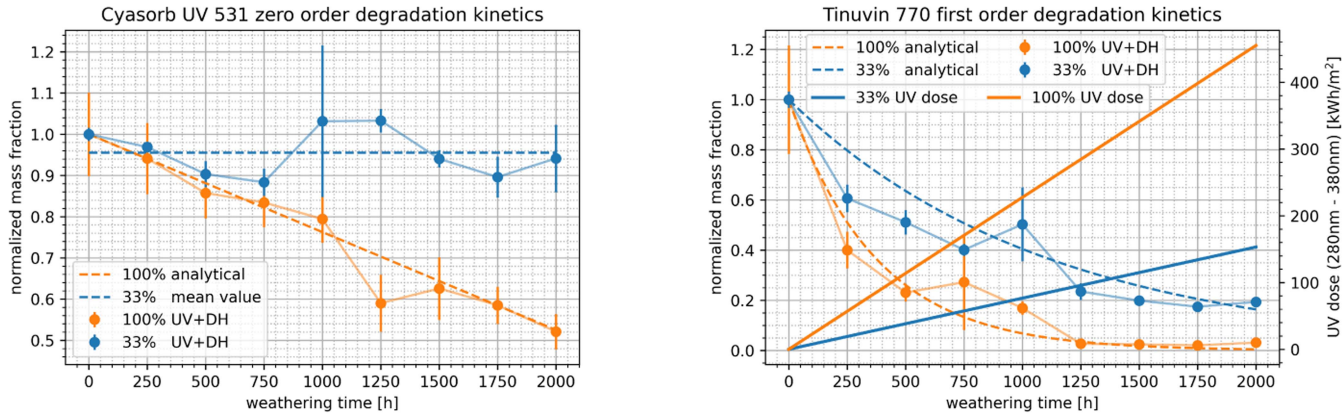

Fig. 2. UV additive quantification of the plain EVA films. Degradation kinetics of the UV absorber Cyasorb UV 531 (left) and the UV stabilizer Tinuvin 770 (right) and the corresponding integrated UV dose between 280 and 380 nm in dependence of the weathering time.

of measurements. The EL measurements were carried out with a greateyes LumiSolar Professional system. A cooled GE2048 512 BI MID CCD sensor is installed in the camera. For the EL measurements, the modules were powered with 8.5 A.

2) Pyrolysis-Gas Chromatography-Mass Spectrometry: For qualitative and quantitative analysis of the polymer and the additive composition, a combination of pyrolysis, gas chromatography, and mass spectrometry (PY-GCMS) was used. The PY-GCMS setup and settings are explained in detail in our previous works focusing on additive quantification [14], [35]. An EGA/Py-3030D from Frontier Laboratories, Ltd., pyrolysis oven with attached autosampler AS-1020E was used for thermo desorption. As gas chromatograph, a Trace 1300 from Thermo Scientific with He carrier gas was used. The implemented column was an Ultra ALLOY Capillary Column (length 30 m, internal diameter 0.25 mm, and film thickness 0.25 μm) from Frontier Laboratories, Ltd. An ISQ 7000 mass spectrometer from Thermo Scientific was coupled to the gas chromatograph. The m/z range was set from 29 to 800.

3) Attenuated Total Reflectance—Fourier-Transform Infrared Spectroscopy: An Inventio spectrometer from Bruker was used for the FTIR analysis. The measurements were carried out in ATR mode using a transit platinum unit with a diamond tip. The wavelength interval was set from 4000 to 650 cm^{-1} with a resolution of 2 cm^{-1} and eight scans.

III. Results and Discussion

A. UV Additive Consumption in Plain EVA Films

As stated in our previous work, the consumption of the UV stabilizer could be a potential marker for the degradation of solar modules [34]. However, the degradation behavior of UV additives in EVA films is currently not fully understood. Consequently, the consumption of the commonly used UV additives Cyasorb UV 531 (UV absorber) and Tinuvin 770 (UV stabilizer) was first investigated as a function of different radiation intensities in laminated EVA films. The degradation kinetics of both additives and the applied UV dose is visualized in Fig. 2. It must be mentioned that only the HALS base molecule can be detected with the PY-GCMS method used. All nitroxide forms resulting from the Denisov cycle remain unaffected by the analysis [38]. It is, therefore, a measure of how quickly the base molecule is consumed under given environmental conditions.

Analyzing the consumption of the UV absorber, a clear difference between both irradiation conditions is observable. For the 33% intensity, the UV absorber amount fluctuates around the mean value and no trend in degradation is observed. This indicates reversible keto-enol tautomerism [16], [39], [40]. In our previous work, we also found that similar intensities will not lead to the decomposition of the UV absorber [13], [14]. However, the 100% weathering shows a continuous decrease of UV absorber concentration until reaching approximately 52% of the initial concentration after 2000 h. This contrasts with the results of Pern [15] who reported an exponential degradation rate of Cyasorb UV 531 in cyclohexane, but in accordance with the work of Pickett and Moore[41], who reported zero-order degradation kinetics of Cyasorb UV 531 in PMMA films. In the case of the carried out weathering, the degradation kinetics of the UV absorber concentration N_C can be described by

$$\frac{\mathrm{d}N_C(t)}{\mathrm{d}t} = -IB_C(\varphi, T) \cdot \Theta(I) \tag{1}$$

with the UV intensity I and a chamber parameter B_C, which is dependent on the relative humidity φ and the temperature T and the Heaviside function Θ, which enables the degradation when a specific intensity threshold is passed. Equation (1) does not contain a dependence on the UV absorber amount $N_C(t)$ because the linear decrease of the mass fraction suggests a degradation kinetic, which is independent of the UV absorber concentration. Thus, (1) can be easily integrated and using the normalized initial condition $N_C(0) = 1$ yields

$$N_C(t) = 1 - IB_C(\varphi, T)t \cdot \Theta(I). \tag{2}$$

Using (2) with $B_C(\varphi, T) = 5.21 \times 10^{-6}$ m^2/J and $I = 227.53$ W/m^2 as integrated UV dose between 280 and 380 nm will lead to the displayed curve. However, the high intensity of the 100% weathering is unrealistic indicating that the UV absorber should not be consumed under outdoor irradiation.

In contrast to the UV absorber, the UV stabilizer degrades under both weathering conditions. This can be explained by the principle of work of the HALS functional groups. They react in the complex Denisov cycle trapping radicals; thus, they

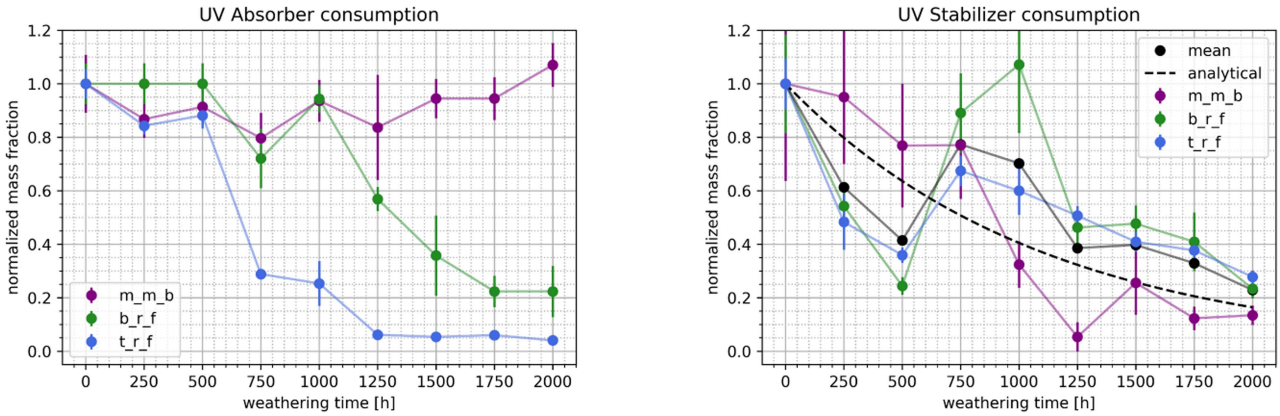

Fig. 3. UV additive quantification of the weathered mini modules. Left: Normalized development of the UV absorber content in dependence of weathering time while the standard deviation of the different samples is represented with the error bar. Right: Normalized development of UV stabilizer content at different positions with standard deviation as error bars, the mean curve of all positions and the analytical curve of (4) with the same chamber parameter as for the plain EVA films. The minimodules were aged with the 33% weathering conditions.

need a reaction partner and will be consumed in dependence of radical presence [38], [42], [43], [44]. The significantly higher consumption under the 100% weathering suggests an increased radical formation compared to the 33% weathering. For the 100% weathering, the HALS base form is nearly completely consumed after 1250 h, whereas for the 33% weathering, there is still about 20% of the base concentration present after 2000 h.

As observed in our previous work, the base form of the UV stabilizer is consumed exponentially [13], [14]. The exponential dependence can be explained by a reservoir effect. Assuming there is a reservoir of radicals for the HALS amines to react with, the decay is only dependent on the amount of HALS molecules $N_T(t)$ (pseudo first-order kinetics). This leads to

$$\frac{\mathrm{d}N_T(t)}{\mathrm{d}t} = -N_T I B_T(\varphi, T) \tag{3}$$

with the UV intensity I and the chamber parameter B_T. Using the normalized initial condition $N_T(0) = 1$ will lead to

$$N_T(t) = e^{-IB_T(\varphi,T)t}. \tag{4}$$

Using (4), the two UV intensities I_{33} and I_{100} and the molecule amounts $N_{T_{33}}$ and $N_{T_{100}}$ for the 100% and 33% weathering, the chamber parameter can be calculated analytically by

$$B_T(\varphi, T) = -\frac{\ln(N_{T_{33}} N_{T_{100}})}{(I_{33} + I_{100})\tilde{t}} \tag{5}$$

while the molecule amount of a specific time point $\tilde{t}$ must be evaluated. Using $B_T(\varphi, T) = 3.28 \times 10^{-9}$ m^2/J, $I_{100} = 227.53$ W/m^2 and $I_{33} = 76.60$ W/m^2 will lead to the displayed curves of the analytic solution of (4). Thus, for fixed humidity and temperature, the consumption of the UV stabilizer can be described sufficiently as a function of the UV intensity.

This can be observed, for example, at the measuring points of both curves for a radiation dose of approximately 120 kWh/m^2. This dose is reached after approximately 1500 h of 33% weathering and leads to a UV stabilizer concentration of approximately 20% of the initial concentration. With 100% weathering, this dose is reached after approximately 500 h and also leads to a UV stabilizer concentration of approximately 20%.

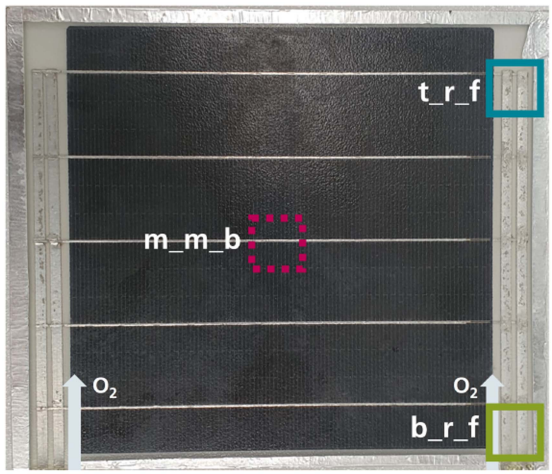

Fig. 4. Exemplary minimodule with encapsulant extraction point. The blue rectangle corresponds to the front EVA on top of the inner interconnector at the top of the module (t_r_f), the green rectangle corresponds to the front EVA on top of the inner interconnector at the bottom of the module (b_r_f) and the purple rectangle corresponds to the back EVA in the middle of the module (m_m_b). The arrows symbolize a possible oxygen pathway at the electrical connectors.

B. *Spatially Resolved Solar Module Degradation*

1) UV Additive Degradation: Minisolar modules have been aged under the same chamber conditions as the previously analyzed polymer films. The data of the 100% weathering were previously analyzed but are further evaluated and compared with the more realistic 33% weathering of this study [34]. An exemplary module with the encapsulant extraction points and the later used abbreviations is displayed in Fig. 4. The corresponding additive consumption in dependence of the weathering time for the 33% weathering is displayed in Fig. 3. The color code of the different positions is in accordance with Fig. 4.

Investigating the degradation behavior of the UV absorber in solar modules in comparison with the plain EVA films shows clear differences. In our previous works, dealing with coupon samples and for the plain EVA samples before, the UV absorber content stayed approximately constant or was fluctuating around the mean value due to inhomogeneities between different

samples [13], [14]. The same behavior can be observed for the backside sample of the module (m_m_b). However, for the front side of the module, the UV absorber content is significantly consumed. Especially for the top side of the module (t_r_f), the content is nearly completely vanished after 1250 h reaching only about 5% of the initial concentration.

As discussed in the weathering section, the temperature between the different positions within the module should be similar, only varying by ± 2 °C. Thus, the diverging behavior of front and back Cyasorb UV 531 consumption is most likely not the result of a temperature effect, because the temperature between front encapsulant and back encapsulant as well as the temperature of plain EVA is only minimally varying. Furthermore, it was shown that the moisture ingress of permeable backsheets is occurring 2-D for the whole backsheet area [45], [46]. Consequently, the m_m_b position should be penetrated by moisture at first, but this does not affect the UV absorber content. It is conceivable that the moisture diffused in over a certain period of time in combination with the UV radiation at positions b_r_f and t_r_f has led to the degradation of the UV absorber. The pure EVA films allow moisture to diffuse in and out quickly, but the layered structure of a solar module traps it. In addition, reactions with the electrical connector in combination with the stressors could lead to the observed behavior. The UV absorber could have been radicalized [47], bound to the connectors and, thus, is not desorbing anymore. Reactions of the UV absorber with excess crosslinking peroxide as in our previous work with another encapsulant are unlikely [14], as the encapsulant used here did not show discoloration or UV absorber degradation in any of our other work [13], [48]. At this stage, the exact cause of this degradation reaction is still unclear.

In contrast to the UV absorber, the UV stabilizer in the mini modules behaves similarly as in the plain EVA. Especially, the m_m_b position shows an exponential decrease. After 2000 h the UV stabilizer content decreased to 15%–25% of the initial content in dependence of the sample position. However, inhomogeneities and internal diffusion between the different sample positions and weathering steps probably resulted in the observed fluctuations [14]. Recently, it was found that the consumption of the HALS base molecule is similar for UV weathering and DH weathering under IEC 61215 [48]. Thus, the UV stabilizer content of all positions was combined in the right image of Fig. 3 using the mean value of the investigated positions. The dashed line represents the analytical solution of (4) using the same B_T as for the plain EVA samples. Except for the 750 and 1000 h weathering steps, which also showed the strongest deviations in comparison with the other weathering steps, the HALS consumption behaves similarly in the mini modules and the plain EVA films. Thus, assuming a reservoir of radicals and describing the UV stabilizer content with (4) seems to be sufficient for plain EVA films and EVA in minimodules when weathered under the same conditions.

2) EVA Degradation: The previously examined EVA positions (see Fig. 4) have been further characterized by attenuated total reflectance—Fourier-transform infrared spectroscopy (ATR-FTIR) measurements. The results are displayed in Fig. 5 (the color coding is in accordance with Fig. 4) while the corresponding peaks and functional groups are listed in Table I. As observable in the full spectrum (top left image), the encapsulant shows all characteristic EVA peaks while significant changes due to aging occur mainly in the region of 1800–1500 cm^{-1}. Thus, further evaluation focused on the mentioned wavenumber interval yielding significant differences regarding the EVA degradation in dependence on the observed position. The displayed graphs (except for the full spectrum) are difference plots, subtracting the initial FTIR spectrum after normalization using the 2850-cm^{-1} CH_2 peak.

TABLE I
FTIR ABSORPTION PEAK ASSIGNMENT

waven. [cm^{-1}]	group	excitation
2920	CH_2	stretching vibration (PE)
2850	CH_2	deformation vibration (PE)
1736	C=O	stretching vibration (VA)
1740-1660	C=O	stretching vibration (acetic acid)
1715-1650	C=O	stretching vibration of ketones
1660-1550	C=C	stretching vibration
1465	CH_2	stretching vibration (PE)
1370	CH_3	deformation vibration (VA)
1238	C-O-C	stretching vibration (VA)
1020	C-O-C	stretching vibration (VA)
960	CH	deformation vibration (VA)
770	CH	vibration of vinyl groups (-CH=CH-)
720	CH_2	skeleton rocking vibration (PE)

Intensities belong to the polyethylene (PE) units, the VA units or degradation products of the base polymer. The assignment is in accordance with the work in [13], [14], [18], [20], [21], [51], [52], and [53].

The b_r_f position shows two significant changes. The 1736-cm^{-1} peak is increasing in intensity and broadening suggesting ketone formation. This species can either be formed by Norrish type III reactions induced by photodegradation or during a breakdown reaction of hydroperoxides [19], [20], [49]. The peak with the center at 1570 cm^{-1} is probably the result of UV-induced Norrish type II reactions forming C=C bonds [17], [18], [20], [50]. The t_r_f position shows no ketone formation during aging. However, Norrish type II reactions with resulting C=C bond formation can be observed [17], [18], [20], [50]. Furthermore, the formation of a new C=C peak at 770 cm^{-1} was observed (not shown). The oxidation index (OI) was calculated using the peak ratio of the 1700 cm^{-1} C=O peak integral and the 720 cm^{-1} CH_2 peak integral as carried out in our previous work [13]. The OI development is visualized in Fig. 6. Only the b_r_f position shows a significant OI increase with ongoing weathering time. Thus, the assumed ketone formation for this position is validated. Although Norrish type III reactions or breakdown reactions of hydroperoxides can lead to ketone formation, the latter is more likely because, otherwise, ketones should have also formed at the t_r_f position, which was exposed to the same UV irradiance. The solar modules have not been sealed with aluminum tape at the electrical contacts (see Fig. 4). Consequently, oxygen diffused into the modules via this point and led to the reaction described at the b_r_f position. In accordance with our previous work, all photodegradation effects seem to be pronounced after approximately 1500 h of weathering, when most of the UV stabilizer is consumed (see Fig. 3) [34].

In comparison with the front encapsulant, the m_m_b position behaves differently. The vanishing peak with the center at approximately 1550 cm^{-1} is probably a vibration of NH groups of the HALS in the initial state [52], [54], [55]. This peak has also been reported in our previous work using the same commercial encapsulant [13]. Thus, it does not correlate with encapsulant degradation of the back EVA. However, the changes of the C=O peak from 1770 to 1600 cm^{-1} are probably a result of EVA

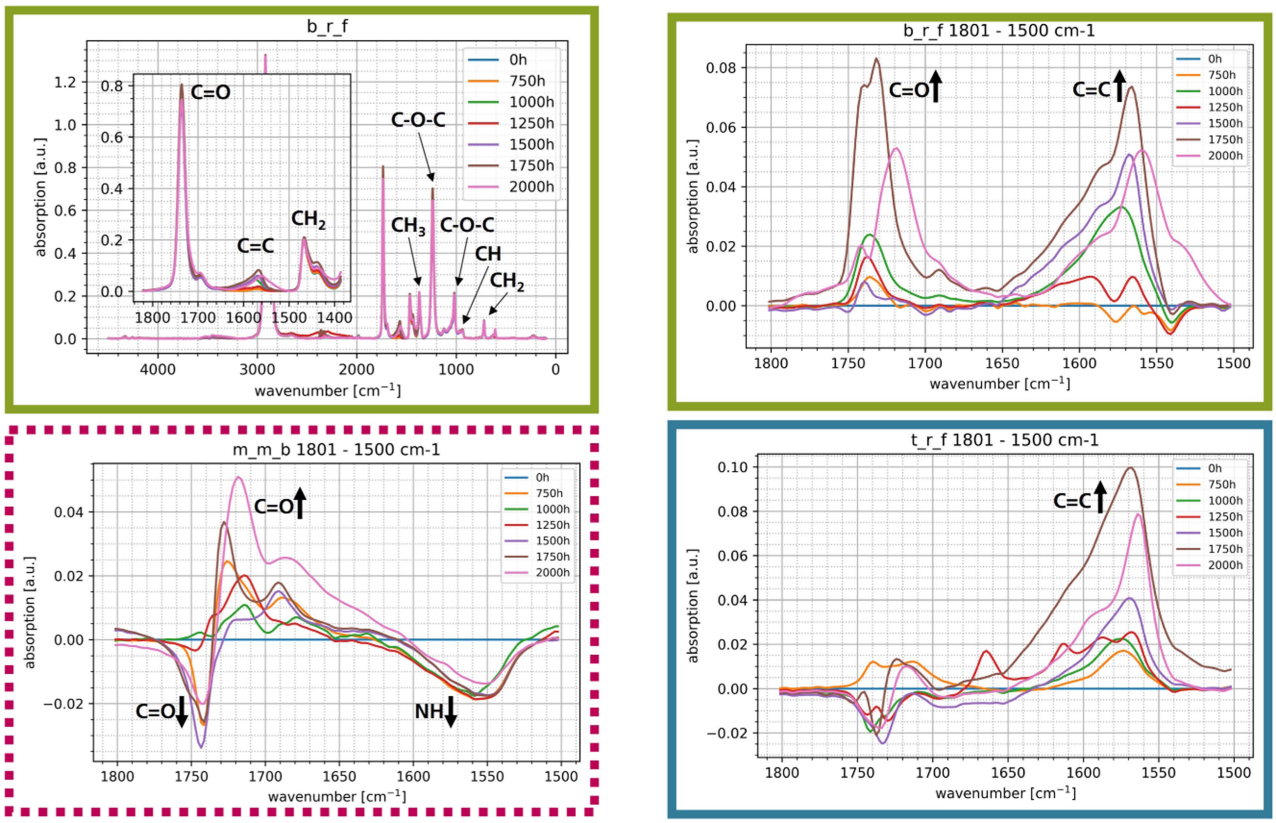

Fig. 5. ATR-FTIR measurements of the examined encapsulant positions. The color coding is in accordance with Fig. 4. The top left image shows a complete FTIR spectrum of the EVA encapsulant. The other images show difference spectra subtracting the initial spectrum after normalization. The minimodules were aged with the 33% weathering conditions.

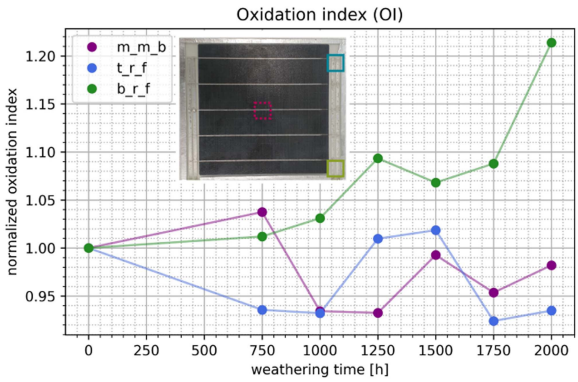

Fig. 6. Oxidation index (ratio of the 1700 cm^{-1} C=O peak integral and the 720-cm^{-1} CH_2 peak integral) in dependence of the position and weathering time. The color code corresponds to Fig. 4. The minimodules were aged with the 33% weathering conditions.

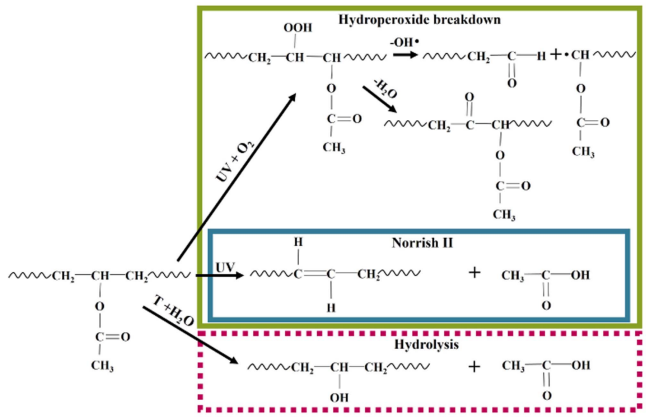

Fig. 7. Observed degradation reactions in dependence of the investigated position. The color code corresponds to Fig. 4. The degradation reactions are based on the work in [17], [18], [20], [27], [28], [49], [50], and [56].

hydrolysis [28], [56]. The decrease in intensity at approximately 1750 cm^{-1} and increase in intensity at approximately 1720 cm^{-1} indicate the formation of acetic acid and were observed for DH aged modules [27], [28]. The measured spectra are also in accordance with the absorbance of pure acetic acid as they show a pronounced C=O peak from 1740 to 1700 cm^{-1}, which can also create a shoulder from 1710 to 1660 cm^{-1} [51]. The UV stabilizer consumption of the m_m_b position is even stronger than for the front encapsulant samples as seen in the Py-GCMS results. For the front EVA, the effect is overlapped with the formation of double bonds observed in the same spectral region. However, as the hydrolysis of EVA does not result in radical formation like for photodegradation, the consumption of the UV stabilizer can probably not easily be correlated to the polymer degradation at this point.

The EVA inside the minimodules degrades differently in dependence of the investigated position and the environmental stressors. Thus, the microclimate at a specific position has a significant impact on the occurring degradation reactions. Fig. 7 visualizes the suggested reactions in dependence of the position

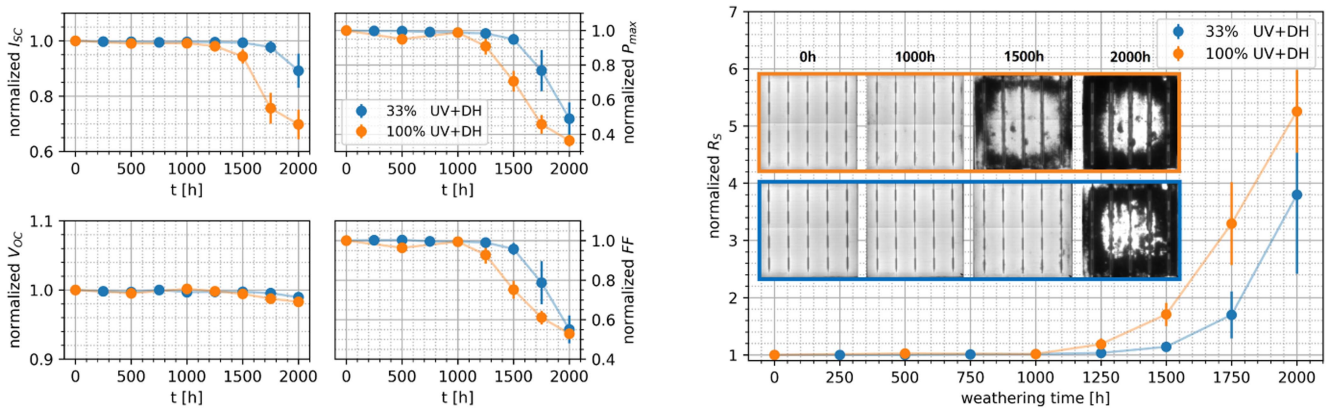

Fig. 8. Development of the electrical key parameters I_{SC}, V_{OC}, P_{max}, and FF (left) and increase in the series resistance R_S in combination with EL measurements (right).

inside the modules. These microclimate effects can possibly intensify for real-sized modules due to different diffusion distances of moisture and additives [14], [45]. Furthermore, they should be highly dependent on the used material combination, especially when combining encapsulant layers with different additive compositions or when using a diffusion-open / diffusion-inhibiting backsheet.

3) Electrical Characterization: The consumption of the UV additives in combination with encapsulant degradation and ingressed moisture led to the degradation of the solar cells. The electrical characterization of both weathering conditions is displayed in Fig. 8 while the comparison with our previous work (100%, orange) is color coded [34]. In comparison with the previous weathering, the 33% weathering shows a comparable behavior of short circuit current (I_{SC}) degradation, open-circuit voltage (V_{OC}) degradation, fill factor (FF) decrease and power decrease at the maximum power point (P_{max}). However, the degradation of all key performance parameters started later, after approximately 1500 h of weathering. Also, the increase in series resistance (R_S) and the decrease in electroluminescence (EL) follow the same pattern but shifted to later times. If Fig. 2 is taken into account, the degradation of the 100% weathering begins after about 230 kWh/m^2 and the degradation of 33% weathering after about 120 kWh/m^2. The combination of irradiation with humidity and temperature, therefore, plays a greater role than the pure UV dose.

While the encapsulant degradation shows a combination of UV (hydroperoxide breakdown and Norrish type II reactions) and DH (hydrolysis) induced degradation, the resulting performance loss of the solar modules can mainly be attributed to the DH effects. As reported by several groups in the literature, the performance loss of PERC-based solar modules induced by UV irradiation is minimal in comparison with the observed degradation [57], [58], [59]. In our previous work, in which we used the same module structure but carried out individual DH and UV weathering, only minimal damage occurred under pure UV aging despite the higher intensity [48]. In particular, FF, which shows a severe decrease, is nearly unaffected by sole UV aging [48], [58], [59].

However, the FTIR analysis showed the hydrolysis of EVA and Norrish type II reactions, both leading to the formation of acetic acid, especially after 1250 h. Thus, the increased R_S that results in a decrease in FF and P_{max} is induced by acetic acid. It was shown in the past that acetic acid corrodes electrical contacts of the solar cells, which leads to an increase in R_S and decrease in EL [60], [61], [62]. In accordance with the literature, this corrosion manifests itself macroscopically first in a drop in FF and in a second step with a reduction in I_{SC} [63]. This is due to the fact that the acetic acid dissolves the Ag-nanoparticles contained in the glass layer between the busbar and the cell [62], [63].

As shown in our previous work, the macroscopic degradation (e.g., performance loss) starts, when most of the UV stabilizer is consumed [34]. The UV stabilizer reached approximately 40% of the initial concentration after 1250 h of weathering, which is just before a significant decrease in the electrical parameters occurred. Although there is no direct link between UV stabilizer consumption and performance losses in the module, the behavior of the UV stabilizer is directly linked to the degradation of the encapsulant. Consequently, the degradation behavior of the UV stabilizer could be used to make assumptions about the expected solar module degradation, as this can be described using (4) or modifications of it.

The used DH conditions (85 °C and 60% r.h.) have a much smaller r.h. than the parameters used in the literature and the weathering standard IEC 61215; however, the examined modules show a significant faster degradation than in the literature [29], [61], [64]. Although the temperature is comparable and the UV irradiance inflicts only minor damage to the solar cell [36], [37], the combination of DH and UV weathering seems to be more severe for the solar modules than DH weathering with higher r.h. This can be explained by the fact that UV-induced Norrish type II reactions also produce acetic acid [18], [20]. Under normal UV aging conditions (low r.h.) there is little moisture available in the module. The acetic acid cannot dissociate and be transferred to all the locations by moisture. Furthermore, the autocatalytic effect is prevented when all the moisture in the module has been used up for hydrolysis [60].

Under combined conditions, after moisture diffusion around the cell [45], [46], sufficient moisture is also available for the acetic acid formed by UV radiation. Consequently, the damage to the modules is greater, although the individual conditions are less

intense than for sole UV weathering or sole DH weathering. This could also explain why the reduction in EL is particularly strong at the edges. The acetic acid produced by EVA hydrolysis can quickly reach the front and back contacts of the solar cell at these positions. Especially at the edges, this effect is superimposed with acetic acid formation due to UV-induced Norrish type II reactions. This means that the front and back contacts are more severely damaged at the edges than in the center, as the acetic acid (or moisture) has to travel a long diffusion path to the front contact in the center of the cell. In the field, however, it is always to be expected that more than one stressor will act simultaneously. This shows a further advantage for the use of the UV stabilizer as a degradation marker. The additive reacts to all forms of stressors, so that modeling is possible under different aging conditions.

IV. Conclusion

The degradation of solar modules is a complex process of various reactions and interactions between the different materials used. It has been shown that the degradation reactions at different points within a module can differ significantly depending on the prevailing microclimate. The UV additives, which are intended to protect the encapsulant from degradation, play a special role here. The UV absorber, which is not consumed in a pure foil, degrades quickly within solar modules if exposed to UV irradiance. On the other hand, the UV stabilizer follows pseudo first-order degradation kinetics, regardless of whether it is embedded in a pure film or in an encapsulant in the module. The derived analytical solution allows one to predict the consumption of the UV stabilizer depending on the used irradiance. Since the degradation behavior of the encapsulant is directly coupled to the consumption of the UV stabilizer base molecule, its degradation kinetics are suitable for modeling macroscopic module degradation.

The combination of UV and DH weathering conditions used caused significant damage to the modules within 1500 h, although the combination of conditions is milder than it would be in the respective individual parameters under IEC 61215. This is probably due to a synergy effect of the Norrish type II reactions with moisture penetration and the hydrolysis of the encapsulant. Both types of reaction lead to the formation of acetic acid, which corrodes the contacts of the solar cell and increases the series resistance. However, the combination of different stressors in the field is a realistic scenario. Consequently, future tests should consider that the combination of stressors can drastically accelerate the degradation behavior of solar modules. In addition, it was found that the hydrolysis of EVA has critical consequences for module reliability compared to photodegradation. Thus, stabilization against hydrolysis by means of suitable additives should be considered.

Although this work dealt with EVA as an encapsulant, various findings are transferable to novel polyolefin elastomer (POE)-based encapsulants. These use the same UV additives, so the UV stabilizer could also be used here for modeling. Furthermore, photo oxidation is also problematic for POE encapsulants, so that the influence of microclimates and the material combination of backsheet and encapsulant used can lead to different degradation reactions at different points within the solar modules.

Acknowledgment

The authors would like to thank Marius Lüdemann for his help with sample preparation.

References

[1] F. J. Nijsse et al., "The momentum of the solar energy transition," *Nature Commun.*, vol. 14, no. 1, 2023, Art. no. 6542.
[2] D. C. Jordan, C. Deline, S. R. Kurtz, G. M. Kimball, and M. Anderson, "Robust PV degradation methodology and application," *IEEE J. Photovolt.*, vol. 8, no. 2, pp. 525–531, Mar. 2018.
[3] A. B. Subramaniyan, R. Pan, J. Kuitche, and G. TamizhMani, "Quantification of environmental effects on PV module degradation: A physics-based data-driven modeling method," *IEEE J. Photovolt.*, vol. 8, no. 5, pp. 1289–1296, Sep. 2018.
[4] I. Kaaya, M. Koehl, A. P. Mehilli, S. de Cardona Mariano, and K. A. Weiss, "Modeling outdoor service lifetime prediction of PV modules: Effects of combined climatic stressors on PV module power degradation," *IEEE J. Photovolt.*, vol. 9, no. 4, pp. 1105–1112, Jul. 2019.
[5] J. Ascencio-Vásquez, I. Kaaya, K. Brecl, K.-A. Weiss, and M. Topič, "Global climate data processing and mapping of degradation mechanisms and degradation rates of PV modules," *Energies*, vol. 12, no. 24, 2019, Art. no. 4749.
[6] B. Brune et al., "Quantifying the influence of encapsulant and backsheet composition on PV-power and electrical degradation," *Prog. Photovolt.: Res. Appl.*, vol. 31, pp. 716–728, 2023.
[7] M. Halwachs et al., "Statistical evaluation of PV system performance and failure data among different climate zones," *Renewable Energy*, vol. 139, pp. 1040–1060, 2019.
[8] A. P. Patel, A. Sinha, and G. Tamizhmani, "Field-aged glass/backsheet and glass/glass PV modules: Encapsulant degradation comparison," *IEEE J. Photovolt.*, vol. 10, no. 2, pp. 607–615, Mar. 2020.
[9] D. C. Jordan, N. Haegel, and T. M. Barnes, "Photovoltaics module reliability for the terawatt age," *Prog. Energy*, vol. 4, no. 2, 2022, Art. no. 022002.
[10] G. Oreski et al., "Motivation, benefits, and challenges for new photovoltaic material & module developments," *Prog. Energy*, vol. 4, no. 3, 2022, Art. no. 032003.
[11] A. Omazic et al., "Relation between degradation of polymeric components in crystalline silicon PV module and climatic conditions: A literature review," *Sol. Energy Mater. Sol. Cells*, vol. 192, pp. 123–133, 2019.
[12] A. Jentsch, K.-J. Eichhorn, and B. Voit, "Influence of typical stabilizers on the aging behavior of EVA foils for photovoltaic applications during artificial UV-weathering," *Polym. Testing*, vol. 44, pp. 242–247, 2015.
[13] R. Heidrich et al., "UV lamp spectral effects on the aging behavior of encapsulants for photovoltaic modules," *Sol. Energy Mater. Sol. Cells*, vol. 266, 2024, Art. no. 112674.
[14] R. Heidrich, M. Lüdemann, A. Mordvinkin, and R. Gottschalg, "Diffusion of UV additives in ethylene-vinyl acetate copolymer encapsulants and the impact on polymer reliability," *IEEE J. Photovolt.*, vol. 14, no. 1, pp. 131–139, Jan. 2024.
[15] F. Pern, "Factors that affect the EVA encapsulant discoloration rate upon accelerated exposure," *Sol. Energy Mater. Sol. Cells*, vol. 41, pp. 587–615, 1996.
[16] F. Pern, "Ethylene-Vinyl acetate (EVA) encapsulants for photovoltaic modules: Degradation and discoloration mechanisms and formulation modifications for improved photostability," *Die Angewandte Makromolekulare Chemie, Appl. Macromol. Chem. Phys.*, vol. 252, no. 1, pp. 195–216, 1997.
[17] A. Czanderna and F. Pern, "Encapsulation of PV modules using ethylene vinyl acetate copolymer as a pottant: A critical review," *Sol. Energy Mater. Sol. Cells*, vol. 43, no. 2, pp. 101–181, 1996.
[18] N. S. Allen, M. Edge, M. Rodriguez, C. M. Liauw, and E. Fontan, "Aspects of the thermal oxidation, yellowing and stabilisation of ethylene vinyl acetate copolymer," *Polym. Degradation Stability*, vol. 71, no. 1, pp. 1–14, 2000.
[19] M. Çopuroğlu and M. Şen, "A comparative study of UV aging characteristics of poly (ethylene-co-vinyl acetate) and poly (ethylene-co-vinyl acetate)/carbon black mixture," *Polymers Adv. Technol.*, vol. 16, no. 1, pp. 61–66, 2005.

[20] J. Jin, S. Chen, and J. Zhang, "UV aging behaviour of ethylene-vinyl acetate copolymers (EVA) with different vinyl acetate contents," *Polym. Degradation Stability*, vol. 95, no. 5, pp. 725–732, 2010.

[21] C. Barretta, G. Oreski, S. Feldbacher, K. Resch-Fauster, and R. Pantani, "Comparison of degradation behavior of newly developed encapsulation materials for photovoltaic applications under different artificial ageing tests," *Polymers*, vol. 13, no. 2, 2021, Art. no. 271.

[22] N. Kim et al., "Study on the degradation of different types of backsheets used in PV module under accelerated conditions," *Sol. Energy Mater. Sol. Cells*, vol. 120, pp. 543–548, 2014.

[23] M. Knausz et al., "Degradation of photovoltaic backsheets: Comparison of the aging induced changes on module and component level," *J. Appl. Polym. Sci.*, vol. 132, no. 24, 2015, Art. no. 42093.

[24] A. Fairbrother, N. Phillips, and X. Gu, "Degradation processes and mechanisms of backsheets," in *Durability and Reliability of Polymers and Other Materials in Photovoltaic Modules*. Amsterdam, The Netherlands: Elsevier, 2019, pp. 153–174.

[25] V. Naumann et al., "Explanation of potential-induced degradation of the shunting type by Na decoration of stacking faults in Si solar cells," *Sol. Energy Mater. Sol. Cells*, vol. 120, pp. 383–389, 2014.

[26] F. ibne Mahmood and G. TamizhMani, "Impact of different backsheets and encapsulant types on potential induced degradation (PID) of silicon PV modules," *Sol. Energy*, vol. 252, pp. 20–28, 2023.

[27] K. Hara, S. Jonai, and A. Masuda, "Crystalline SI photovoltaic modules functionalized by a thin polyethylene film against potential and damp-heat-induced degradation," *RSC Adv.*, vol. 5, no. 20, pp. 15017–15023, 2015.

[28] K. Hara and Y. Chiba, "Spectroscopic investigation of long-term outdoor-exposed crystalline silicon photovoltaic modules," *J. Photochemistry Photobiol. A, Chem.*, vol. 404, 2021, Art. no. 112891.

[29] *Terrestrial Photovoltaic (PV) Modules - Design Qualification and Type Approval - Part 2: Test Procedures*, IEC Standard 61215-2:2021, *Int. Electrotechnical Commission, Geneva, Switzerland*, 2021.

[30] *Measurement Procedures for Materials Used in Photovoltaic Modules - Part 7-2: Environmental Exposures - Accelerated Weathering Tests of Polymeric Materials*, DIN IEC/TS 62788-7-2, Int. Electrotechnical Commission, Geneva, Switzerland, 2019.

[31] D. E. Mansour et al., "Effect of backsheet properties on PV encapsulant degradation during combined accelerated aging tests," *Sustainability*, vol. 12, no. 12, 2020, Art. no. 5208.

[32] M. Owen-Bellini et al., "Advancing reliability assessments of photovoltaic modules and materials using combined-accelerated stress testing," *Prog. Photovolt. Res. Appl.*, vol. 29, no. 1, pp. 64–82, 2021.

[33] P. Hacke et al., "Acceleration factors for combined-accelerated stress testing of photovoltaic modules," *Sol. RRL*, vol. 7, no. 12, 2023, Art. no. 2300068.

[34] R. Heidrich, A. Mordvinkin, and R. Gottschalg, "Spatially resolved degradation analysis of solar modules after combined accelerated aging," in *Proc. IEEE 50th Photovolt. Specialists Conf.*, 2023, pp. 1–3.

[35] R. Heidrich, A. Mordvinkin, and R. Gottschalg, "Quantification of UV protecting additives in ethylene-vinyl acetate copolymer encapsulants for photovoltaic modules with pyrolysis-gas chromatography-mass spectrometry," *Polym. Testing*, vol. 118, 2023, Art. no. 107913.

[36] J. Pickett, D. Gibson, S. Rice, and M. Gardner, "Effects of temperature on the weathering of engineering thermoplastics," *Polym. Degradation Stability*, vol. 93, no. 3, pp. 684–691, 2008.

[37] J. E. Pickett and J. R. Sargent, "Sample temperatures during outdoor and laboratory weathering exposures," *Polym. Degradation Stability*, vol. 94, no. 2, pp. 189–195, 2009.

[38] J. L. Hodgson and M. L. Coote, "Clarifying the mechanism of the Denisov cycle: How do hindered amine light stabilizers protect polymer coatings from photo-oxidative degradation ?," *Macromolecules*, vol. 43, no. 10, pp. 4573–4583, 2010.

[39] N. A. Shaath, "Ultraviolet filters," *Photochemical Photobiological Sci.*, vol. 9, pp. 464–469, 2010.

[40] J. Zawadiak and M. Mrzyczek, "Influence of substituent on UV absorption and keto–enol tautomerism equilibrium of dibenzoylmethane derivatives," *Spectrochimica Acta Part A, Mol. Biomol. Spectrosc.*, vol. 96, pp. 815–819, 2012.

[41] J. E. Pickett and J. E. Moore, "Photodegradation of UV absorbers: Kinetics and structural effects," *Die Angewandte Makromolekulare Chemie: Appl. Macromol. Chem. Phys.*, vol. 232, no. 1, pp. 229–238, 1995.

[42] E. Denisov, "The role and reactions of nitroxyl radicals in hindered piperidine light stabilisation," *Polym. Degradation Stability*, vol. 34, no. 1–3, pp. 325–332, 1991.

[43] E. N. Step, N. J. Turro, P. P. Klemchuk, and M. E. Gande, "Model studies on the mechanism of HALS stabilization," *Die Angewandte Makromolekulare Chemie, Appl. Macromol. Chem. Phys.*, vol. 232, no. 1, pp. 65–83, 1995.

[44] M. R. Paine, G. Gryn'ova, M. L. Coote, P. J. Barker, and S. J. Blanksby, "Desorption electrospray ionisation mass spectrometry of stabilised polyesters reveals activation of hindered amine light stabilisers," *Polym. Degradation Stability*, vol. 99, pp. 223–232, 2014.

[45] M. Jankovec et al., "In-situ monitoring of moisture ingress in PV modules using digital humidity sensors," *IEEE J. Photovolt.*, vol. 6, no. 5, pp. 1152–1159, Sep. 2016.

[46] M. Jankovec, S. Mitterhofer, J. Slapšak, and M. Topič, "Monitoring of lateral moisture ingress across the surface of a solar cell in PV modules," in *Proc. 47th IEEE Photovolt. Specialists Conf.*, 2020, pp. 1308–1312.

[47] P. Klemchuk et al., "Investigation of the degradation and stabilization of EVA-based encapsulant in field-aged solar energy modules," *Polym. Degradation Stability*, vol. 55, no. 3, pp. 347–365, 1997.

[48] R. Heidrich et al., "From performance measurements to molecular level characterization: Exploring the differences between UV and DH weathering of PV modules," *Sol. RRL*, vol. 8, 2024, Art. no. 2400144.

[49] M. Gardette et al., "Photo-and thermal-oxidation of polyethylene: Comparison of mechanisms and influence of unsaturation content," *Polym. Degradation Stability*, vol. 98, no. 11, pp. 2383–2390, 2013.

[50] M. C. C. de Oliveira, A. S. A. D. Cardoso, M. M. Viana, and V. D. F. C. Lins, "The causes and effects of degradation of encapsulant ethylene vinyl acetate copolymer (EVA) in crystalline silicon photovoltaic modules: A review," *Renewable Sustain. Energy Rev.*, vol. 81, pp. 2299–2317, 2018.

[51] G. Socrates, *Infrared and Raman Characteristic Group Frequencies: Tables and Charts*. Hoboken, NJ, USA: Wiley, 2004.

[52] G. Oreski, G. M. Wallner, and R. Lang, "Ageing characterization of commercial ethylene copolymer greenhouse films by analytical and mechanical methods," *Biosyst. Eng.*, vol. 103, no. 4, pp. 489–496, 2009.

[53] B. Ottersböck, G. Oreski, and G. Pinter, "Comparison of different microclimate effects on the aging behavior of encapsulation materials used in photovoltaic modules," *Polym. Degradation Stability*, vol. 138, pp. 182–191, 2017.

[54] S. Falicki, D. Gosciniak, J. Cooke, and D. Carlsson, "Secondary and tertiary piperidinyl compounds as stabilizers for γ-irradiated polypropylene," *Polym. Degradation Stability*, vol. 43, no. 1, pp. 1–7, 1994.

[55] R. Singh et al., "Synthesis of new polymeric hindered amine light stabilizers: Performance evaluation in styrenic polymers," *J. Appl. Polym. Sci.*, vol. 90, no. 4, pp. 1126–1138, 2003.

[56] M. Patel et al., "Thermal stability of poly (ethylene-co-vinyl acetate) based materials," *Polym. Testing*, vol. 32, no. 4, pp. 785–793, 2013.

[57] R. Witteck et al., "UV-induced degradation of PERC solar modules with UV-transparent encapsulation materials," *Prog. Photovolt. Res. Appl.*, vol. 25, no. 6, pp. 409–416, 2017.

[58] A. Sinha et al., "UV-induced degradation of high-efficiency silicon PV modules with different cell architectures," *Prog. Photovolt., Res. Appl.*, vol. 31, no. 1, pp. 36–51, 2023.

[59] U. Desai, B. K. Sharma, and A. Singh, "Assessment of the effect of accelerated ultraviolet aging on mini-PV modules encapsulated with different poly (ethylene-co-vinyl acetate) formulations," *J. Appl. Polym. Sci.*, vol. 140, no. 45, 2023, Art. no. e54676.

[60] M. D. Kempe et al., "Acetic acid production and glass transition concerns with ethylene-vinyl acetate used in photovoltaic devices," *Sol. Energy Mater. Sol. Cells*, vol. 91, no. 4, pp. 315–329, 2007.

[61] C. Peike et al., "Origin of damp-heat induced cell degradation," *Sol. Energy Mater. Sol. Cells*, vol. 116, pp. 49–54, 2013.

[62] A. Kraft et al., "Investigation of acetic acid corrosion impact on printed solar cell contacts," *IEEE J. Photovolt.*, vol. 5, no. 3, pp. 736–743, May 2015.

[63] M. Köntges et al., *Assessment of Photovoltaic Module Failures in the Field: International Energy Agency Photovoltaic Power Systems Programme: IEA PVPS Task 13, Subtask 3: Report IEA-PVPS T13-09: 2017*. Paris, France: Int. Energy Agency, 2017.

[64] M. Koehl, S. Hoffmann, and S. Wiesmeier, "Evaluation of damp-heat testing of photovoltaic modules," *Prog. Photovolt. Res. Appl.*, vol. 25, no. 2, pp. 175–183, 2017.